JOURNAL OF COMPUTATIONAL PHYSICS 80, 204–231 (1989)

The Equilibrium Flux Method for the Calculation of Flows with Non-equilibrium Chemical Reactions

M. N. MACROSSAN

Department of Mechanical Engineering, University of Queensland, Australia

Received August 21, 1987; revised February 8, 1988

The equilibrium flux method (D. I. Pullin, *J. Comput. Phys.* **34**, 231 (1980)) is a kinetic theory based finite volume method for calculating the flow of a compressible ideal gas. It is shown here that, in effect, the method solves the Euler equations with added pseudo-dissipative terms and that it is a natural upwinding scheme. The method can be easily modified so that the flow of a chemically reacting gas mixture can be calculated. Results from the method for a one-dimensional non-equilibrium reacting flow are shown to agree well with a conventional continuum solution. Results are also presented for the calculation of a plane two-dimensional flow, at hypersonic speed, of a dissociating gas around a blunt nosed body.

1. INTRODUCTION

Pullin [1] proposed a direct simulation method, derived from the kinetic theory of gases, for the calculation of a flow of a compressible gas. Another kinetic theory based method, due to Reitz [2], has been applied to two-dimensional flows by Deshpande [3] but Pullin's equilibrium flux method or EFM has not been taken up. Because they are derived from the physical modelling of a flow at a molecular level these kinetic theory methods have some characteristics which make them promising candidates for the calculation of flows about hypersonic cruise or re-entry vehicles, where the flow energy is great enough to initiate chemical reactions in air. Both methods automatically ensure, with no complicated logic, that physical signals are transmitted in the correct directions and, in particular, in the hypersonic limit EFM becomes an upwind scheme (see Appendix). Both methods lend themselves naturally to the inclusion of finite rate chemical reactions by a simple de-coupling of the fluid dynamics and chemical equilibriating processes. A similar de-coupling has been used to calculate elliptic internal reacting flows by Greenberg and Presser [4]. They discuss the advantages of such an approach, namely that all the stiffness of the governing partial differential equations, which arises from the different chemical reaction rates, appears in a system of ordinary differential equations which can be solved by Gear's standard technique [5]. For two-dimensional flows Pullin's EFM has an advantage over Reitz's method in that it is a finite volume scheme which can be applied on unstructured grids. The

0021-9991/89 $3.00

Cartesian co-ordinate formulation of Reitz's method seems to make it more difficult to apply to arbitrary boundary shapes.

Because EFM is derived directly from considerations of the physics of the flow, rather than the governing equations, it is difficult to classify the method, but it is shown in the Appendix that it may be considered as a finite volume solution method for the Euler equations with added terms. These "pseudo-dissipative" terms arise naturally from the physical simulation of the flow at a molecular level and, unlike an aritificial viscosity term, cannot be adjusted to provide the desired degree of smoothness in the solution. It appears, however, that it is this pseudo-dissipation which makes EFM particularly robust. The lack of robustness of traditional methods for the Euler equations has led the authors of Ref. [6] to use Godunov's method for the calculation of supersonic flows about complex body shapes even though some price in terms of accuracy and computer time was incurred. Unlike Godunov's method, EFM requires no iteration at each time step and thus may be preferable. EFM is an explicit time stepping method and is subject to a limitation on the time step to ensure stability. With the stability condition satisfied, EFM produces no unphysical oscillations near shocks. This is an important feature since such oscillations would be expected to produce disastrous effects on chemically reacting flows where the reaction rates are extremely sensitive to changes in temperature.

The equilibrium flux method was derived from Bird's direct simulation Monte Carlo (DSMC) method [7]. The latter method follows, at a molecular level the evolution of the distribution $f(\mathbf{v}, \mathbf{x}, t)$ of molecular velocities $\mathbf{v}$ by a direct computer simulation of molecular motions and collisions in a network of cells representing the flowfield. It yields [8] a statistical solution of the Boltzmann equation,

$$\frac{\partial}{\partial t}[nf] + \mathbf{v}\frac{\partial}{\partial \mathbf{x}}[nf] = \left\{\frac{\partial}{\partial t}[nf]\right\}_{\text{coll}}, \tag{1}$$

where n is the number density, which describes the evolution of f. The Euler equations may be derived from the Boltzmann equation by considering the infinite collision rate limit in which the local molecular velocity distribution everywhere conforms to the local equilibrium or Maxwellian distribution

$$f(\mathbf{v}) = (\beta/\pi^{1/2})^3 \exp[-\beta^2 \mathbf{c}^2], \tag{2}$$

where $\mathbf{c} = \mathbf{v} - \mathbf{u}$ is the molecular thermal velocity, $\mathbf{u} = \bar{\mathbf{v}}$ is the mean molecular velocity (or local flow velocity), $\beta^{-1} = (2RT)^{1/2}$ is the most probable molecular thermal speed, R is the gas constant, and T is the local temperature. The equilibrium flux method is the infinite collision rate or equilibrium limit of DSMC.

In the following sections DSMC is briefly described as an introduction to EFM. Then EFM is described in detail, first for an inert gas mixture and then for a chemically reacting gas. Results of calculations for a one-dimensional flow problem, the propagation of a plane normal shock in a reacting gas, are then presented. For

simplicity, calculations were made for only one chemical reaction, although any number of reactions may in theory be included. The single reaction was the dissociation reaction

$$A_2 = A + A,$$

where A_2 denotes a diatomic molecule made up of two atoms of element A. As a further simplification, the chemical dynamics are represented by Lighthill's [9] ideal dissociating gas and its associated reaction rate equation proposed by Freeman [10]. These EFM calculations are compared with an exact solution obtained by integrating the governing equations behind a shock wave. Finally the results of some two-dimensional calculations of a high speed flow of a dissociating gas about a blunt-nosed body are shown and compared with the results of independent calculations of a similar flow.

2. The Direct Simulation Method

In DSMC the behaviour of a rarefied gas is studied by calculating the motions of some thousands of "simulator molecules" which represent the molecules of the gas. To make this feasible the molecular collisions and the free flight between collisions are treated separately, and alternatively, for a series of short time steps.

The flowfield is divided into small cells of characteristic length smaller than the local molecular mean free path and the simulator molecules are moved in collisionless trajectories for a short time Δt carrying from cell to cell their mass, momentum, and energy. After the molecules have moved, it is assumed that each cell is isolated from other cells while the molecular velocities are changed by calculating representative collisions amongst the molecules in each cell. The number of collisions in the interval Δt must be such that the local collision rate is correct. In the next step the molecules move according to the velocities established by the collisions. Since the molecular velocities are known throughout the flow at each step, the local flow properties, which are assumed to be constant over each cell, can be obtained from the sample of molecules in that cell.

3. The Equilibrium Flux Method

In DSMC the effect of the collisions is to drive the distribution of molecular velocities towards the equilibrium distribution given by (2). In the limit of an infinite collision rate the distribution of molecular velocities everywhere would tend asymptotically towards the equilibrium distribution determined by the total mass, momentum, and energy within a cell. If the velocity distribution were known to be given by (2) the fluxes of mass, momentum, and energy which would be carried from cell to cell by the simulator molecules could be calculated. It turns out

therefore that in this infinite collision rate or equilibrium limit of the direct simulation method there is no need for simulator molecules.

In the equilibrium flux method [1] the total mass, momentum, and energy in each cell are stored and these, with the cell volumes, determine the local density, mean velocity, and temperature, all of which are assumed to be constant within each cell. Given that the molecular velocity distribution is Maxwellian, the fluxes of mass, momentum, and energy across a cell boundary in a short time Δt can be calculated from straightforward kinetic theory assuming free molecular flight. These amounts are deducted from the cell and added to the mass, momentum, and energy in the cell sharing this boundary. The return flux across the boundary is calculated from the conditions in the adjacent cell or, at solid boundaries, the flow is reflected. At fluid boundaries the fluxes pass out of the flowfield and incoming fluxes are calculated according to the boundary conditions. After the fluxes have been calculated, the new amounts of mass, momentum, and energy in each cell determine the new local density, mean velocity, and temperature and these in turn determine the fluxes in the next time step. If Δt is less than the time it takes the flow to traverse a cell, that is if $V_c \Delta t/\Delta x < 1$, where V_c is a representative local fluid or signal speed and Δx is the cell size, it can be assumed that the fluxes flow between adjacent cells only. If Δt is not small it is found that the calculation is unstable. In other words the CFL number must be less than one. The calculation can begin with freestream conditions in each cell, and then proceeds as the unsteady solution of an impulsively started flow until steady conditions are reached.

3.1. *The Equilibrium Flux Quantities*

Figure 1 shows a cell in which the stream (mean) velocity is inclined at an angle θ to one of the cell boundaries. The fluxal quantities (/unit time/unit area) in one direction across this boundary are required for an equilibrium gas. They are [7]:

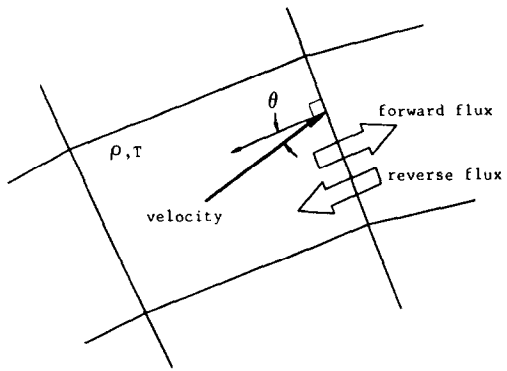

FIG. 1. A typical cell exchanges fluxes of mass, momentum, and energy with a neighbouring cell across the common boundary.

for mass

$$(\rho/\beta)[\exp(-s_n^2) + \pi^{1/2} s_n H(s_n)]/(2\pi^{1/2}) \tag{3a}$$

for normal momentum

$$(\rho/\beta^2)[s_n \exp(-s_n^2) + \pi^{1/2} H(s_n)\{\tfrac{1}{2} + s_n^2\}]/(2\pi^{1/2}) \tag{3b}$$

for tangential momentum

$$(\rho/\beta^2)\, s_p[\exp(-s_n^2) + \pi^{1/2} s_n H(s_n)]/(2\pi^{1/2}) \tag{3c}$$

for translational energy

$$(\rho/\beta^3)[(s^2+2)\exp(-s_n^2) + \pi^{1/2} s_n H(s_n)\{s^2 + 5/2\}]/(4\pi^{1/2}) \tag{3d}$$

for energy in molecular structure

$$(\rho/\beta)\, e_{\text{st}}[\exp(-s_n^2) + \pi^{1/2} s_n H(s_n)]/(2\pi^{1/2}), \tag{3e}$$

where $s = \beta u$ is the speed ratio, $s_n = s\cos\theta$, $s_p = s\sin\theta$, $H(s_n) = 1 + \text{erf}(s_n)$, and e_{st} is the energy stored in the structure of the molecule. If ξ is the number of active degrees of freedom of the molecular structure then

$$e_{\text{st}} = \xi RT/2. \tag{4}$$

The internal energy of the gas, which includes the random or thermal part of the translation energy, is $e_{\text{int}} = \frac{1}{2}(3+\xi)\, RT$ and the ratio of specific heats is $\gamma = (5+\xi)/(3+\xi)$. For a gas mixture the calculations must be based on an "average" molecule. In this case, or if some energy modes are not fully excited, ξ may not be an integer.

The density ρ, stream velocity $\mathbf{u}$, and temperature T in a cell of volume V may be determined from the mass M, momentum (P_x, P_y), and energy E in that cell as follows:

$$M = \rho V \tag{5a}$$

$$P_x = Mu_x \tag{5b}$$

$$P_y = Mu_y \tag{5c}$$

$$E = M[\tfrac{1}{2}u^2 + e_{\text{int}}]. \tag{5d}$$

3.2. *Relationship to the Euler Equations*

Provided that the cell size were smaller than the local mean free path, DSMC would produce a solution of the Euler equations in the limit of an infinite collision rate and zero mean free path. Long before such a limit was reached, however, DSMC would become prohibitively expensive in computation time. EFM is a practical alternative but, because of the finite cell size, it provides an approximation

only to this hypothetical limit of DSMC. In EFM the collision part of DSMC has been taken to the limit of an infinite collision rate (that is, the conditions in each cell are assumed to be those corresponding to local kinetic equilibrium), but the corresponding limit of zero mean free path in the convection calculation cannot be achieved. A fluid element must travel a distance approximately equal to the cell size before it can adjust to any flow gradients. Hence there is an effective mean free path in these calculations approximately equal to the cell size. This conclusion can be verified by considering Fig. 2 which shows two adjacent cells in a flow in which there is a gradient du/dy of the flow velocity parallel to the x-axis and the density and temperature in each cell are the same. If the velocities in the cells are u_a and u_b then there is a net flux (/unit area/unit time) of x-momentum across the boundary. The shear stress on the boundary is equal to this net flux and is, from (3c),

$$\tau = \rho(RT/2\pi)^{1/2}(u_b - u_a).$$

Comparing this to the stress–strain relationship for Couette flow,

$$\tau = \mu\, du/dy,$$

and approximating du/dy by $(u_b - u_a)/\Delta y$, where Δy is the distance between the cell centroids, we obtain a pseudo-viscosity for EFM as

$$\mu = (RT/2\pi)^{1/2}\rho\, \Delta y.$$

Comparing this result to the usual relation between mean free path, λ, and viscosity; that is, $\mu = \frac{1}{2}\rho\bar{c}\lambda$, where $\bar{c} = (8RT/\pi)^{1/2}$ is the mean molecular thermal speed, we obtain a pseudo mean free path

$$\lambda = \Delta y/2.$$

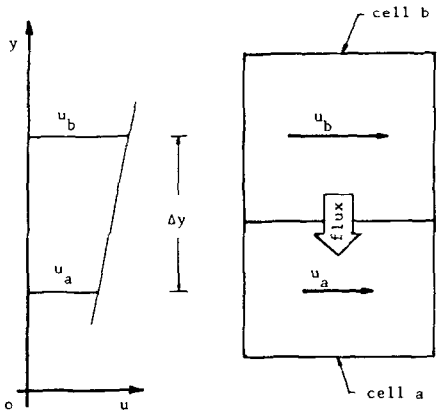

FIG. 2. Adjacent cells in the presence of a velocity gradient exchange momentum, giving rise to a pseudo-viscosity.

A similar analysis for the transport of thermal energy when there is a temperature difference between the cells yields an expression for the coefficient of thermal conductivity. Thus

$$K = (\gamma + 1)\, c_v (RT/8\pi)^{1/2} \rho\, \Delta y.$$

Other pseudo-dissipative effects are present. A density gradient will induce a flow of mass between the cells as will a temperature gradient. These pseudo-dissipative effects are examined in more detail for a one-dimensional flow in the Appendix.

4. Chemical Reactions

If α represents a typical species concentration in a reacting gas mixture the change in concentration is given by $D\alpha/Dt = \partial\alpha/\partial t + \mathbf{u} \cdot \nabla\alpha$, where $D\alpha/Dt$ is the Lagrangian chemical reaction rate which will depend on the local density, temperature, and chemical composition. Chemical reactions are incorporated into EFM as follows:

(1) The continuous variation with position of chemical composition is represented by a uniform composition within a cell with discontinuities of composition between cells. In addition to the totals of momentum and energy in each cell, the total mass of each chemical species in each cell must be stored.

(2) The chemical reactions are frozen as the cells exchange mass, momentum, and energy. The fluxes are calculated using the appropriate R and ξ for the gas mixture in each cell. The total mass flux across a boundary is divided into separate fluxes of each chemical species.

(3) After the cells exchange mass, momentum, and energy, the chemical composition is changed by calculating an adiabatic reaction for each cell, in which chemical potential energy is converted to thermal energy or vice versa. The reaction in each cell is independent of neighbouring cells, and proceeds for the time Δt, for which the fluxes were calculated, at a rate depending on the conditions in that cell. The new composition gives new values of R and ξ which are used when calculating the next set of fluxes.

In effect, the chemical reactions are de-coupled from the convection calculations in the same way as the collisions and convection are de-coupled in DSMC.

The calculations may begin with freestream conditions in each cell and should continue until the chemical composition in a cell no longer changes over a complete time step.

4.1. *The Dissociation Reaction*

The equation of state for a mixture of molecules A_2 and dissociated atoms A is $p = \rho(1 + \alpha)\, R_{AA} T$, where $\alpha = [A]/([A] + 2[A_2])$ is the degree of dissociation, and R_{AA} is the gas constant for the diatomic species. That is, the gas constant for the

mixture is $R=(1+\alpha)\,R_{AA}$. The chemical potential energy (the dissociation energy) is $\alpha\theta_D R_{AA}$, where θ_D is the dissociation temperature, a constant for the particular gas. The diatomic component of the ideal dissociated gas has two rotational degrees of freedom and its two vibrational degrees of freedom are always half excited (see [11, p. 159]). The atomic species has energy of translation only and electronic excitation is ignored. For the mixture then, the energy stored in the molecular structure is $e_{st}=\xi RT/2$, where

$$\xi=3(1-\alpha)/(1+\alpha) \tag{6}$$

is the effective number of active degrees of freedom. The specific internal energy, e_{int}, is equal to $(e_{tr}+e_{st}+\alpha\theta_D R_{AA})$ or, (see [11, p. 160]),

$$e_{int}=R_{AA}(3T+\alpha\theta_D). \tag{7}$$

Although the dissociation energy could be calculated from the dissociation at any time, it is convenient to calculate the transport of dissociation energy from cell to cell. To do this it is necessary to replace e_{st} in Eq. (3e) by $e_{st}+\alpha\theta_D R_{AA}$. The total energy in a cell will then include the dissociation energy.

After the fluxes have been calculated, the next step is to determine the change in composition brought about by allowing the dissociation reaction to run for a time Δt. For this adiabatic reaction both α and T vary, subject to the condition that e_{int} is constant. The constant internal energy in each cell can be found from Eq. (5d).

The rate equation proposed by Freeman [10] for the ideal dissociating gas is

$$D\alpha/Dt=\rho CT^{\eta}[(1-\alpha)\exp(-\theta_D/T)-\rho/\rho_D\alpha^2]. \tag{8}$$

The characteristic density, ρ_D, is constant for a particular gas, and C and η are constants which can be found by matching the reaction rate (8) to the usual reaction rates $k_1=2\alpha C_1 T^{\eta_1}\exp(-\theta_D/T)$ and $k_2=(1-\alpha)\,C_2 T^{\eta_2}\exp(-\theta_D/T)$ for the reactions

$$A_2+A \overset{k_1}{=} 2A+A$$

and

$$A_2+A_2 \overset{k_2}{=} 2A+A_2.$$

The result (see [11, p. 233]) is

$$WCT^{\eta} \doteq 2\alpha C_1 T^{\eta_1}+(1-\alpha)\,C_2 T^{\eta_2},$$

where W is the molecular weight of the diatomic species. The constants C and η should be selected to make the correspondence as close as possible for the range of temperatures and degree of dissociation being considered.

Equations (7) and (8) can be combined to give the differential equation describing the reaction as either $\partial\alpha/\partial t = F(\alpha)$ or $\partial T/\partial t = G(T)$, one of which must be solved for each cell at each time step to yield α and T after a time Δt. A Runge–Kutta technique, described in Ref. [12, p. 129], was used to solve these equations. The errors in α and T are related by

$$\left|\frac{\Delta\alpha/\alpha}{\Delta T/T}\right| = e_{\text{int}}/\alpha\theta_D R_{AA} - 1.$$

The fractional error for α is greater than for T when $2\alpha < \alpha_{\max}$, where $\alpha_{\max} = e_{\text{int}}/\theta_D R_{AA}$. In this case the equation $\partial\alpha/\partial t = F(\alpha)$ is solved. Otherwise the equation $\partial T/\partial t = G(T)$ is solved.

5. Dissociation behind a Plane Shock

As a test of EFM, a plane one-dimensional shock can be produced by simulating the action of a shock tube. At time $t = 0$ a flowfield, consisting of a number of cells of equal length, is filled with a gas which is at rest. This gas is bounded by a specularly reflecting surface at one end and at the other end by an interface with a "driver" gas which has a speed U_p. For $t > 0$, the boundary with the driver gas moves into the rest gas with the speed U_p and produces a shock which travels through the test gas. The density, chemical composition, and temperature of the driver gas must be the same as the values of these quantities in the test gas when chemical equilibrium is reached behind the shock. In other words, once chemical equilibrium is achieved behind the shock, the moving interface separates the two gases which are both at rest with respect to the boundary and have the same density, chemical composition, and temperature. In this case the boundary condition is the same as that produced by a specularly reflecting surface or "piston" moving at speed U_p into the test gas. However, until chemical equilibrium is reached behind the shock, the total amount of mass within the flowfield can change. If it could not change then some disturbance of the density profile, like that noted in Ref. [1], would be expected. Such a disturbance would have an unpredictable effect on the chemical reaction and is best avoided.

Because the length of the flowfield decreases as the computation progresses and the number of cells within the flowfield is constant, the boundaries between cells move at different speeds. The fluxes from cell to cell across these moving boundaries can be found from Eqs. (3), using the velocity of the fluid relative to the boundary to calculate the speed ratio. This yields the amounts of momentum $\Delta p'$, and energy $\Delta E'$ (both referred to the axes moving with the boundary), and the amount of mass Δm which are transferred between cells. Before being added to or subtracted from the quantities of momentum and energy in the cells, both $\Delta p'$ and $\Delta E'$ must be

converted to quantities relative to the global co-ordinate system. The necessary transformations are

$$\Delta p = \Delta p' + \Delta m U_b \tag{9a}$$

$$\Delta E = \Delta E' + \tfrac{1}{2}\Delta m U_b^2 + \Delta p' U_b, \tag{9b}$$

where U_b is the boundary speed and Δp and ΔE are the transported momentum and energy referred to the global axes.

Calculations were made for a Mach 15 shock propagating through oxygen, for which $\rho_D = 150\,\text{g/cc}$ [9] and $\theta_D = 59380\,\text{K}$ [13], at a temperature of approximately 237 K and a density of 1.5×10^{-5} g/cc, conditions which correspond roughly to those in the earth's atmosphere at an altitude of 32 km. For these calculations the reaction rate constants for the ideal dissociating gas were taken as $C = 1 \times 10^{26}$ (in c.g.s. units) and $\eta = -3.0$, which give a reasonable representation of the variation of the reaction rate for oxygen (Ref. [13]) for the conditions ranging from those immediately behind the shock to those far downstream.

Table I shows the preshock conditions (denoted by the subscript 1), the conditions which would be expected behind the shock if the dissociation reaction were frozen (denoted by the subscript f), and the equilibrium conditions far behind the shock (denoted by the subscript 2). These last were found by an iterative solution of the conservation equations, the equation of state, and the condition

$$\alpha_2^2/(1-\alpha_2) = \rho_D/\rho_2 \exp(-\theta_{\mathcal{D}}/T_2) \tag{10}$$

for chemical equilibrium for the ideal dissociated gas. The boundary or piston velocity required to produce the shock is

$$U_p = u_1 - u_2. \tag{11}$$

Figure 3 shows the density profile, which is moving from right to left, at successive times after the calculation begins. The x-axis shows the distance along the shock tube as a fraction of its original length, L, which in this case was 1.5 cm.

TABLE I

Pre-shock	Behind chemically frozen shock	Chemical equilibrium behind shock
$\rho_1 = 10^{-7}\rho_D$	$\rho_f/\rho_1 = 6.8182$	$\rho_2/\rho_1 = 12.8324$
$\frac{1}{2}u_1^2/R_{AA}\theta_D = 0.6$	$u_f/u_1 = 0.1467$	$u_2/u_1 = 0.0779$
$R_{AA}T_1/u_1^2 = 1/300$	$R_{AA}T_f/u_1^2 = 0.1256$	$R_{AA}T_2/u_1^2 = 0.0542$
$M_1 = 15.0$	$M_f = 0.1904$	$M_2 = 0.2415$
$\alpha_1 = 0.0$	$\alpha_f = 0.0$	$\alpha_2 = 33.07\%$

$\rho_D = 150$ g/cc, $\theta_D = 59{,}380$ K, $C = 10^{26}$, $\eta = -3.0$

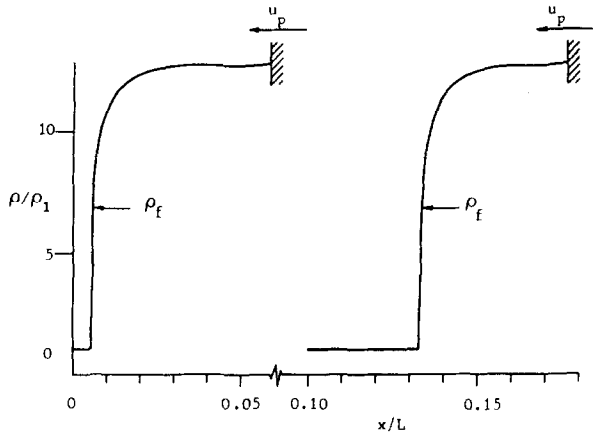

FIG. 3. The density profiles of a dissociating gas in an ideal shock tube at two different times. The shock is driven by the interface which moves from right to left. There are 500 cells in the flowfield. The initial length of the shock-tube was 1.5 cm.

The flowfield was divided into 500 cells. In this calculation, and all the following 1D calculations, the time interval Δt at any step was set equal to $\frac{1}{2}\Delta x/u_1$, where Δx was the current size of a cell.

The density expected behind the Mach 15 shock if the dissociation reaction were frozen is marked in the figure and it can be seen that the density rises sharply to this value. As dissociation proceeds, thermal energy is removed from the flow and the density increases further until, far behind the shock, the dissociation has virtually reached equilibrium. Then the density profile undulates slightly near its equilibrium value.

It can be seen in the Appendix that, because of the pseudo-dissipative effects, the continuum fluxes of mass, energy, and momentum, evaluated for conditions at the cell centroids, are different from the calculated fluxes across cell boundaries wherever there are flow gradients. In the frame of reference in which the shock is stationary, it is the fluxes across the cell boundaries which, in the steady state, are the same throughout the flow and equal to the continuum fluxes evaluated upstream of the shock. It follows that the conditions in each cell cannot satisfy the conservation equations where there are flow gradients. In these calculations the deviation was as much as 20% within the shock and as little as 1% or 2% downstream of the shock.

In theory, equilibrium is reached only infinitely far behind the shock, so the undulation in the density profile may be a downstream boundary effect of the finite length of the flowfield in these calculations. To determine if this has any serious effect closer to the shock, the results for the EFM calculations can be compared with the results obtained with the following analytical solution for the flow of the ideal dissociating gas behind the shock.

5.1. *Analytical Solution*

For this flow, in the steady state, the Lagrangian derivative $D\alpha/Dt$ reduces to $u\, d\alpha/dx$. Therefore, from (8), the dissociation behind the shock, as a function of distance, is a solution of the differential equation

$$d\alpha/dx = Q(\alpha), \tag{14a}$$

where

$$Q(\alpha) = \rho C T^{\eta}\{(1-\alpha)\exp(-\theta_D/T) - \rho/\rho_D \alpha^2\}/u \tag{14b}$$

and for a given value of α the state variables ρ, u, and T may be found as follows:

The conservation equations which ρ, u, and T must satisfy are

$$\Psi_1 = \rho u \tag{15}$$

$$\Psi_2 = \rho u^2 + \rho(1+\alpha)\, R_{AA} T \tag{16}$$

$$\Psi_3 = \tfrac{1}{2}u^2 + R_{AA}[\alpha\theta_D + (4+\alpha)\, T], \tag{17}$$

where Ψ_1, Ψ_2, and Ψ_3 are constants evaluated from the known conditions upstream of the shock. The second term in (17) is the specific enthalpy for the ideal dissociating gas. Equations (15) and (16) can be combined to yield

$$\Psi_2 = \Psi_1\{u^2 + (1+\alpha)\, R_{AA} T\}/u. \tag{18}$$

Since (17) can be rearranged to yield the velocity as a function of T, (18) can be written as

$$g(T) = 0, \tag{19a}$$

where

$$g(T) = \Psi_2 - \Psi_1\{u^2 + (1+\alpha)\, R_{AA} T\}/u \tag{19b}$$

and

$$u = [2\{\Psi_3 - R_{AA}(\alpha\theta_D + (4+\alpha)T)\}]^{1/2}. \tag{19c}$$

Equation (19) can be solved iteratively using Newton's method to yield the temperature corresponding to the degree of dissociation behind the shock. Once T is known the remaining state variables can be found from the conservation equations, and the function $Q(\alpha)$ can be evaluated. Equation (14) can thus be integrated to yield

$$x = \int_0^{\alpha} \{Q(\alpha)\}^{-1}\, d\alpha \tag{20}$$

TABLE II

Initial length of flowfield cm	Final length of flowfield $\bar{x}$	Number of cells	CPU (s) IBM3083E	Ω Eq. (21a), based on final cell length Δx
30	27.0	400	260	0.305
20	17.7	500	330	0.160
10	8.86	500	250	0.8×10^{-1}
6.5	5.76	500	250	0.52×10^{-1}
3.0	2.70	400	220	0.305×10^{-1}
1.5	1.31	500	330	0.118×10^{-1}
2.0	1.74	1000	1320	0.788×10^{-2}
0.6	0.552	500	430	0.5×10^{-2}
0.5	0.640	700	930	0.29×10^{-2}
0.6	0.552	1000	1590	0.25×10^{-2}
0.6	0.552	2000	6030	0.125×10^{-2}
0.6	0.511	3000	15060	0.77×10^{-3}

which relates the degree of dissociation to the distance downstream of the shock. The integration of (20) was performed numerically using a quadrature routine described in Ref. [12, p. 97].

5.2. *Analytical and EFM Results Compared*

A number of calculations using different numbers of cells and different initial lengths of the flowfield were made and are summarised in Table II. The results from one such calculation are shown in Fig. 4, where the solid curve shows the solution

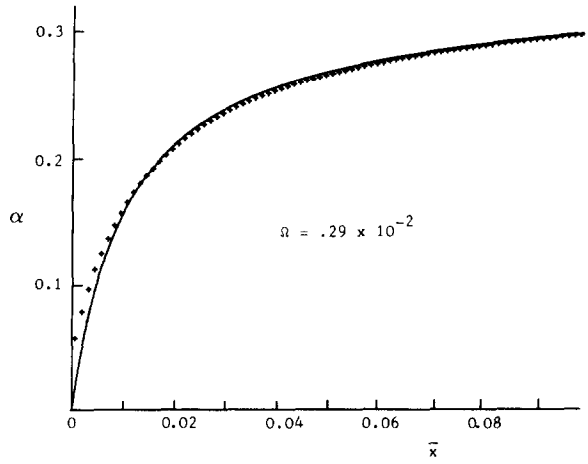

FIG. 4. The profile of the dissociation fraction behind a plane shock in an ideal shock tube. The solid line is the solution of Eq. (20). The crosses show the EFM results in every second cell. The flowfield extends beyond the range shown and consists of 700 cells.

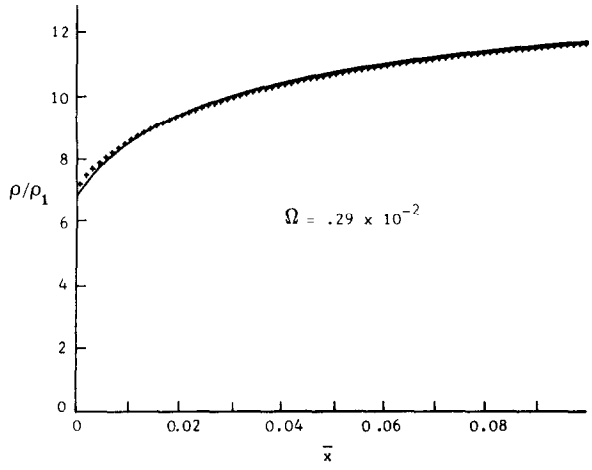

FIG. 5. Density profile. See Fig. 4 for key.

of (20) for the dissociation profile behind the shock. The dimensionless length scale is $\bar{x} = x\rho C/R_{AA}^{\eta} u_1^{1-2\eta}$. The results for the EFM calculation are shown as crosses and, for the sake of clarity, the results from every second cell only are plotted. In EFM the shock is smeared over a few cells and the dissociation reaction begins within the shock. The initial disturbance is propagated at a speed slightly greater than the theoretical shock speed until it is far from the driving interface. Therefore the exact position of the shock, which is the origin for the length scale, is not uniquely defined but has been set at the point where the density is equal to the expected value of density behind the shock if the reaction were frozen. Except for very near the shock, the EFM calculation gives good results. Figures 5 and 6 show the density and velocity profiles for EFM compared with the profiles derived from

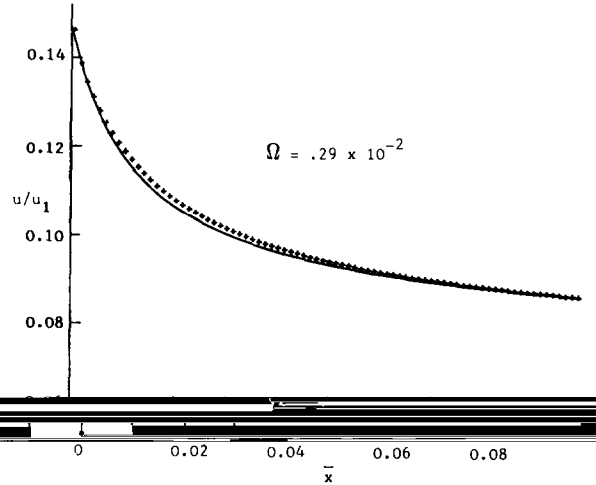

FIG. 6. Velocity profile. See Fig. 4 for key.

the solution of (20). Again the correspondence is good. As already mentioned, the density and velocity profiles for the EFM calculations are not simply connected through the continuity equation. These results suggest that this error is small.

In order to resolve the chemical relaxation, the cell size Δx in these calculations should be small with respect to the characteristic reaction length in the flow. Thus the dimensionless parameter

$$\Omega = (d\alpha/dt)_f(\Delta x/u_1) \tag{21a}$$

should be as small as possible. Here $(d\alpha/dt)_f$ is the rate of Eq. (8) evaluated for the conditions immediately behind the shock, that is, for the conditions in the second column of Table I. In Fig. 7 three profiles of the dimensionless temperature $\bar{T} = R_{AA}T/u_1^2$ behind the shock are shown, as calculated with three different cell sizes, each compared with the analytical solution. The flowfields in these calculations extend far beyond the range shown in the figure (see Table II), but it is only near the shock that the EFM results differ appreciably from the exact solution. The dissociation fraction at the nominal shock position is not zero (see Fig. 4) and therefore the calculated temperature at the shock is less than that shown in the analytical solution. Figure 8 shows how the ratio of the temperature calculated by EFM at the shock to the exact value at the shock approaches unity as the cell size decreases, and also how the temperature calculated just downstream of the shock compares with the exact value at that location. This figure and Fig. 7 show that the error in the calculated temperature is small except very near the shock for a wide range of cell sizes.

These 1D calculations have shown that EFM produces results which approach the exact solution as the cell size is reduced. However, this one-dimensional problem was particularly expensive computationally for EFM (see Table II), since the relaxation region behind the shock which must be resolved extends, in theory, to infinity. Because a uniform cell size was used throughout the flowfield, a large

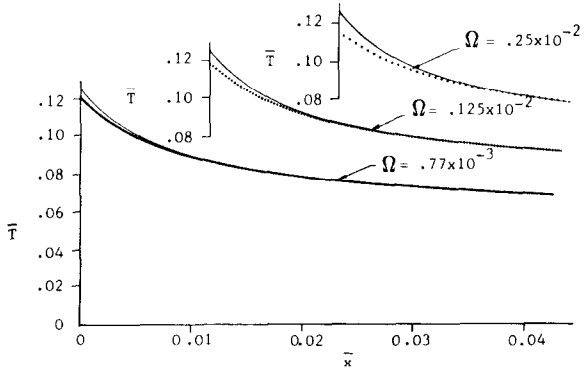

FIG. 7. The effect of cell size in EFM. The crosses show the temperature profile behind the shock for three different cell sizes in the EFM calculations. The solid line is derived from the solution of Eq. (20).

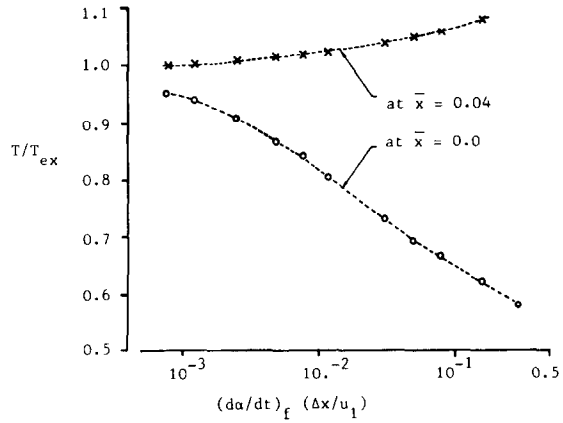

FIG. 8. Approach to the exact solution behind the shock as the cell size Δx decreases, for two different distances from the shock. The temperature calculated by EFM is T. The exact solution is T_{ex}.

number of cells was required to obtain an adequate resolution near the shock. It is very likely that the computer times for these calculations could have been reduced with little effect on the accuracy by using much larger cells in the flow a long way from the shock. In any event the following calculations of the flow of an ideal dissociating gas about a plane two-dimensional blunt body represent a more useful application of the method. Since the downstream boundary condition is supersonic in this case the flowfield can be truncated with negligible danger of affecting the flow upstream.

6. PLANE 2D CALCULATIONS

The plane two-dimensional flow of a dissociating gas around a short blunt body with a semi-cylindrical nose was chosen as a test case for EFM, since results for this type of flow using a different calculation method are available for comparison. These are the results of Hornung [14], who used an inverse method [15] which starts with an assumed shock shape and derives a body shape which, in those calculations, could deviate from being perfectly cylindrical by about 5%. Although he used a more complete model of the chemical dynamics than the ideal dissociating gas used here, his results help to assess qualitatively the behaviour of the present method.

A "general purpose" computer program, able to handle an arbitrary two-dimensional flowfield has been developed. The program constructs the cell network in the way described by Bird [7] for DSMC. The flowfield for this case, divided into cells, is shown in Fig. 9. Two boundaries of the flow, corresponding to the surface of the body and the line of symmetry, were taken as specularly reflecting. The freestream conditions along the upstream boundary were set equal to the pre-shock conditions

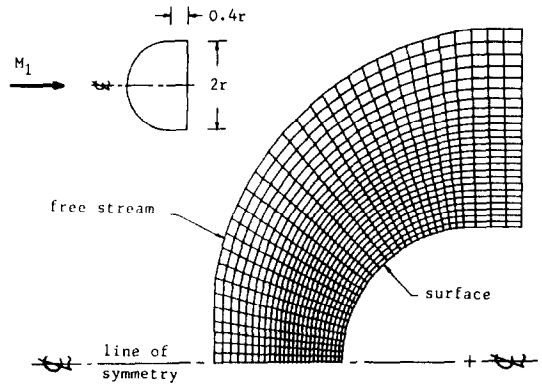

FIG. 9. The flowfield for the blunt body, divided into cells.

shown in Table I. The downstream boundary conditions were determined by assuming there were no gradients of any flow properties across the boundary. Since the flow is supersonic near the downstream boundary, any errors in that boundary condition will have negligible effect upstream.

The ideal dissociating gas with the reaction rate parameters for oxygen given above was used in these calculations. The calculations were performed for values of the nose radius, r, of 0.005 cm and 0.25 cm. Therefore the dimensionless reaction rate parameter based on the nose radius, that is

$$\Omega = (d\alpha/dt)_f(r/u_1) \tag{21b}$$

was 0.218 or 10.9. If r were very small so that Ω tended to zero there would be negligible chemical reaction effects on the flow about the body. Conversely, if Ω were very large, the flow would be everywhere in local chemical equilibrium. This parameter, based on the smallest cell size along the stagnation line, Eq. (21a), was 0.0056 or 0.289. The calculations started from freestream conditions in every cell and proceeded for longer than the time required to achieve virtually steady conditions throughout the flowfield.

Figure 10 shows the streamlines derived from the computational results for the two cases. The sonic line is also shown and the point were it intersects the stagnation streamline was used to determine the approximate shock stand-off distances for the two cases as $\Delta/r = 0.27$ and 0.19. Figure 11 shows these results compared with those obtained by Hornung [14]. The latter results were well correlated for different freestream conditions by the reaction rate parameter Ω, when the stand-off distance was reduced in the form $\frac{1}{2}(\Delta/r)(\rho_f/\rho_1)$. It can be seen that the present results agree reasonably well with those results, given the differences betwen the mathematical models and that the shock position is uncertain in EFM. Figure 12 shows the density contours derived from the EFM calculations and these are similar, except for the finite width of the shock, to those shown in Ref. [14] for similar values of Ω.

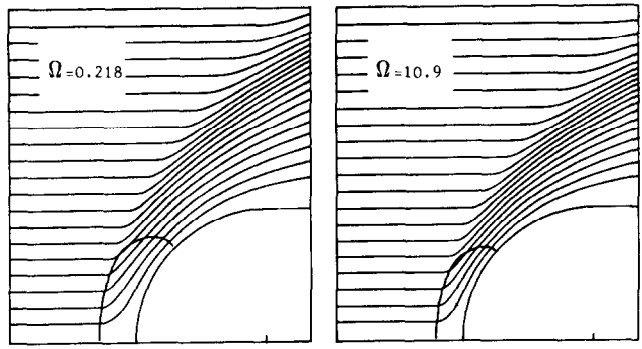

FIG. 10. The streamlines about a blunt body and the sonic line derived from EFM calculations for two different values of the reaction rate parameter. Freestream conditions are in Table I.

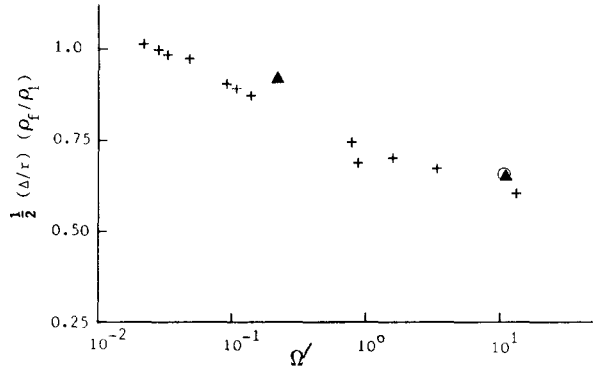

FIG. 11. The shock stand-off distance versus rate parameter. The crosses show the results from Ref. [14]. The triangles show the EFM results for $M = 15$; the circle, for $M = 5.66$.

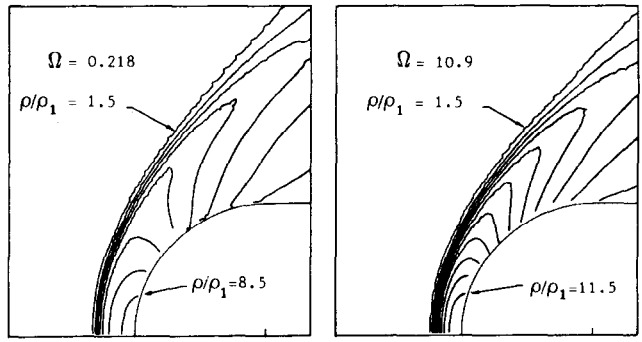

FIG. 12. Equally spaced contours of density for $\rho/\rho_1 = 1.5, 2.5, \ldots$, for two values of the reaction rate parameter. Freestream conditions are in Table I.

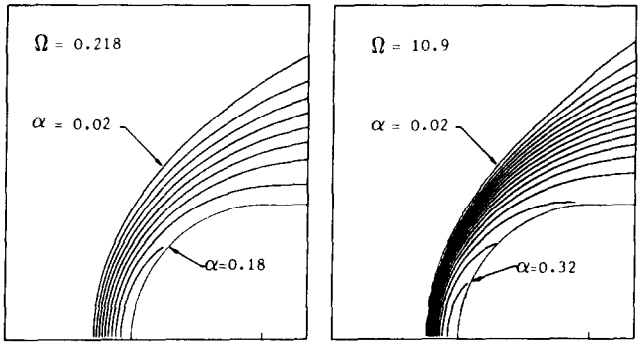

FIG. 13. Equally spaced contours of dissociation for $\alpha = 0.02, 0.04, \ldots$, for two values of the reaction rate parameter. Freestream conditions are in Table I.

In Ref. [14] it was suggested that the distinctive feature of this flow was that the dissociation reaction was in effect frozen behind the shock for most of the flow outside the stagnation region. This was also found with EFM. Figure 13 shows the contours of dissociation obtained with EFM and it can be seen that these contours roughly follow the streamlines in Fig. 10 for a large part of the flow behind the shock.

Further calculations of the flow about a blunt nose were made to determine the sensitivity of EFM to changes in the time step and the cell size. Two additional computational grids were used, both similar to that used before and shown in Fig. 9. Each grid had 43 divisions along the body surface and either 20 or 40 layers of evenly spaced cells in the radial direction. The freestream conditions, shown in Table III, are typical of those in the test section of a shock tube wind tunnel [16] which can produce strong dissociation of nitrogen on a model with a nose radius of $r = 0.5$ cm. For nitrogen $\rho_D = 130$ g/cc, $\theta_D = 113000$ K, $C = 1 \times 10^{26}$, and $\eta = -2.89$. The reaction rate parameters were chosen to represent the reaction rate for nitrogen given in Ref. [13]. The reaction rate parameter (21b) for these

TABLE III

Freestream Conditions

$\rho_1/\rho_D = 3.06 \times 10^{-7}$
$\frac{1}{2}u_1^2/R_{AA}\theta_D = 0.548$
$R_{AA}T_1/u_1^2 = 0.019$
$M_1 = 5.66$
$\alpha_1 = 0.164$
$r = 0.5$ cm

$\rho_D = 130$ g/cc $\quad \theta_D = 113{,}000$ K
$C = 10^{26} \quad \eta = -2.89$

Figure 14 shows iso-Mach lines for the flow calculated on each grid, at a time of $\hat{t}=3.0$ after the impulsive start of the flow. The dimensionless time $\hat{t}$ is equal to $t/r\beta_1$, where the reference speed β_1^{-1} is evaluated for the freestream conditions. The shock is thinner for the finer grid but the general nature of the flow is the same. The shock stand-off distance, again determined from the sonic line, was $\Delta/r=0.26$ for the coarse grid and $\Delta/r=0.25$ for the finer grid. The latter value is plotted in Fig. 11 and agrees well with the results for the Mach 15 flow and reasonably well with the results of Ref. [14].

A quantitative assessment of the sensitivity of EFM to the change in cell size can be made by comparing the pressures acting on the body in the two cases. These pressures can be compared in the form of integrated force co-efficients C_x and C_y given by

$$C_x=\sum p_s\Delta_s \sin\theta/(\tfrac{1}{2}\rho_1 u_1^2 r)$$

$$C_y=-\sum p_s\Delta_s \cos\theta/(\tfrac{1}{2}\rho_1 u_1^2 r).$$

In these equations, Δ_s is the length of a surface element, θ is the angle the surface makes with the x-direction, p_s is the pressure acting on the element and $\frac{1}{2}\rho_1 u_1^2$ is the dynamic pressure in the freestream. The summation extends over all surface cells. The surface pressure was calculated in a manner consistent with the assumptions of EFM. Since in EFM the molecular fluxes are specularly reflected at the surface, the surface pressure is twice the normal momentum flux into the surface given by Eq. (3b) and depends only on the conditions in the cell adjacent to the surface. It may be greater or less than the adjacent fluid pressure if the component of fluid velocity normal to the surface is greater than or less than zero.

Figure 15 shows the time history of the two force co-efficients as calculated on the two grids. Although the figure shows that the body forces are not entirely independent of the grid, the differences are less than 0.2% and 0.75% for C_x and

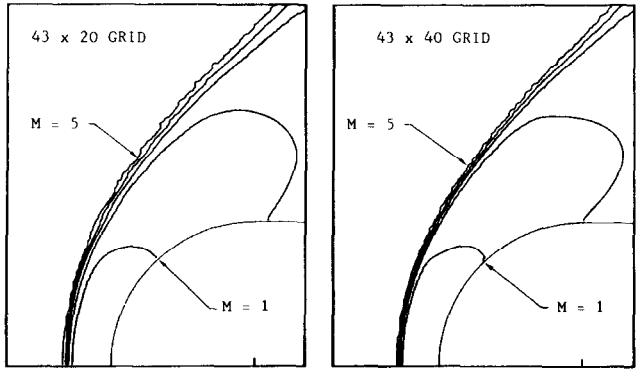

FIG. 14. Equally spaced iso-Mach lines as calculated on two grids. Freestream conditions are in Table III.

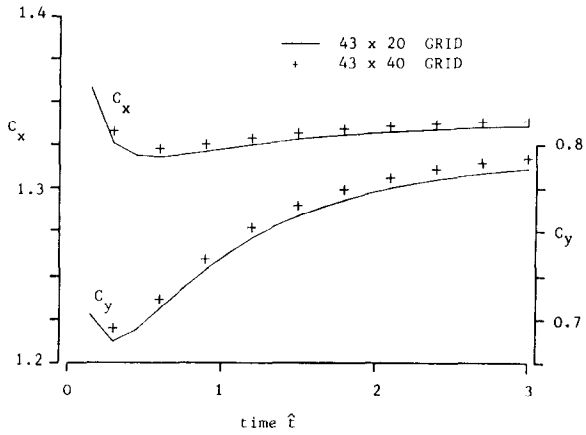

FIG. 15. Time history of the surface force co-efficients as calculated on the two grids. Freestream conditions are in Table III.

C_y, respectively. This figure shows also the rather slow approach to a steady state which is a characteristic of unsteady time-stepping calculations.

These calculations were performed with a constant time step such that the maximum CFL number in the smallest cell was 0.89. The calculations on the coarser grid were repeated with the time step reduced to one-tenth of the previous value. The time histories of the force co-efficients for the two different time steps are compared in Fig. 16. The results are the same to within 0.08% and 0.12% for C_x and C_y, respectively. Iso-Mach lines for the results obtained with the smaller step size were found to be indistinguishable from those in Fig. 14 which were obtained with the larger time step. A shorter calculation, on the finer grid using a time step 10 times smaller, produced iso-Mach lines (not shown here) identical with those obtained at the same elapsed time with the larger time step.

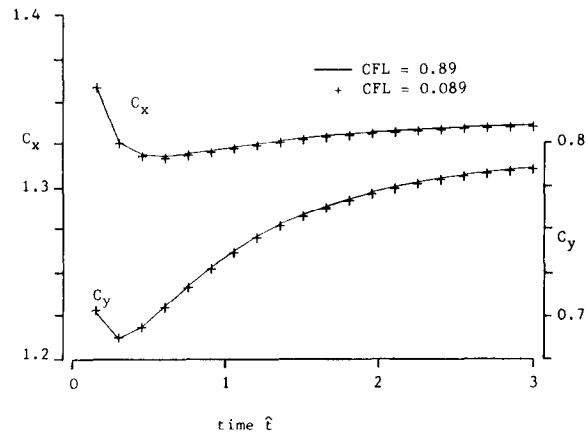

FIG. 16. Time history of the surface force co-efficients on the 43 x 20 grid for different time steps. Freestream conditions are in Table III.

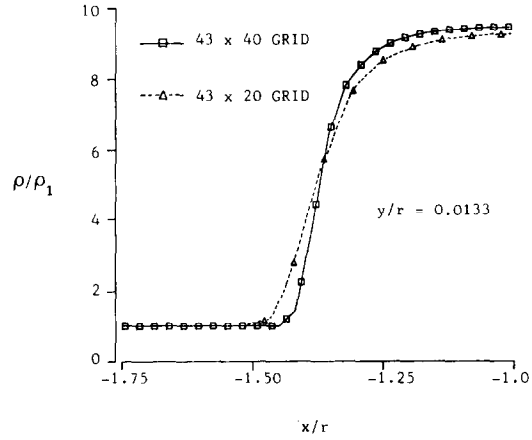

FIG. 17. Near-stagnation line density for two different cell sizes. Freestream conditions are in Table III.

Figure 17 shows the density in the cells adjacent to the stagnation line for the two different grids. As expected the shock is steeper on the smaller grid but its position is virtually unchanged. There is a noticeable difference in density behind the shock although the corresponding profiles of dissociation for the two cases (Fig. 18) show very little difference in this region. Because the dissociation temperature is large, very small changes in dissociation can cause large changes in the temperature and hence the density.

The dissociation profiles along a streamline, which begins at the point $x/r = -1.7$, $y/r = 0.38$ and passes around the blunt nose, are compared in Fig. 19 for the two grids. Very little difference can be seen except that the dissociation falls

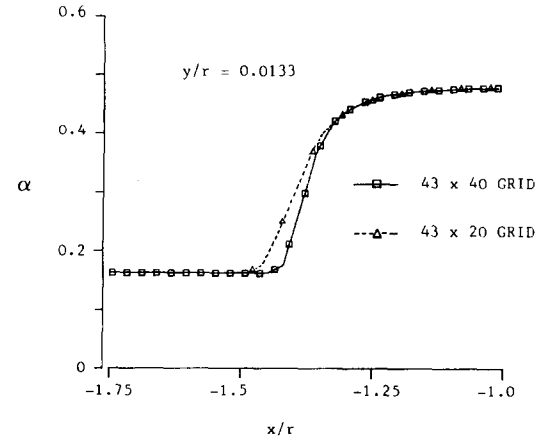

FIG. 18. Near-stagnation line dissociation for two different cell sizes. Freestream conditions are in Table III.

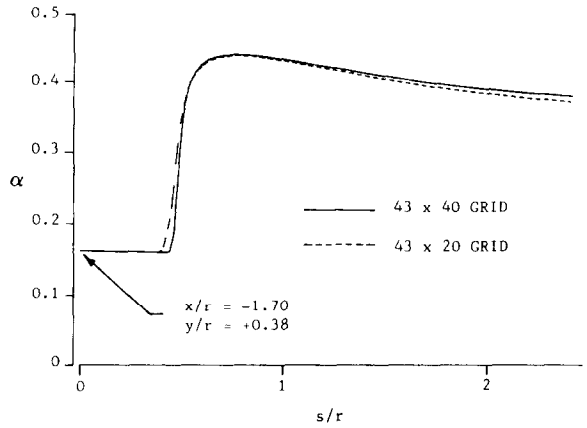

FIG. 19. Dissociation profiles along streamline as calculated on two different grids. Freestream conditions are in Table III.

slightly more rapidly behind the shock for the coarse grid. This difference can be attributed to the pseudo-dissipative effects which are related to the different cell sizes in the two calculations. In the steady state the variation of dissociation along a streamline is given by

$$v\, d\alpha/ds = R - d,$$

where R is the local reaction rate from Eq. (8), v is the local velocity, and d represents the pseudo-dissipation (or error) which in the region behind the shock consists primarily of diffusion across the streamlines because of the density gradient in that direction. Figure 20 shows how the pseudo-dissipation, normalised with respect to the maximum dissociation rate in the flow, that is,

$$(R - v\, d\alpha/ds)/(d\alpha/dt)_f,$$

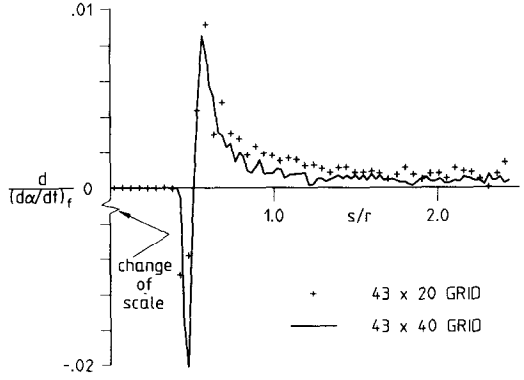

FIG. 20. Pseudo-dissipation along the same streamline as in Fig. 19. Freestream conditions are in Table III.

TABLE IV

Mach number	Ω Eq. (21b)	Grid	$\Delta\hat{t}$	Max CFL	$\hat{t}$ max	CPU (s) IBM3083E
15	0.218	32 × 25	0.0001	0.039	1.64	11,750
15	10.9	32 × 25	0.0001	0.039	1.50	10,090
5.66	10.6	43 × 20	0.006	0.98	3.0	290
5.66	10.6	43 × 20	0.0006	0.098	3.0	2220
5.66	10.6	43 × 40	0.003	0.98	3.0	1030
5.66	10.6	43 × 40	0.0003	0.098	1.8	4300

varies along the streamline for each calculation. Behind the shock it is smaller on the finer grid and in both cases it is much smaller than it is within the shock. Because the local reaction rate is very small behind the shock, the pseudo-dissipation in these calculations is of the same order of magnitude as the reaction rate there. The absolute error, however, is small and the results in Figs. 14, 15, and 19 show that this has a negligible effect on these calculations for practical purposes. However, this does indicate that EFM would be unsuitable for flows in which very slow reactions predominate.

All the CPU times for the two-dimensional calculations, together with the time-step, the maximum CFL number, and the number of cells in the grid, are shown in Table IV. These times apply to an IBM 3083E which runs at approximately 1 MFLOPS. The IBM FORTRAN compiler (version 2.0) with the optimisation level 2 was used. In these calculations the CPU time was almost equally divided between the calculation of the fluid dynamics and the chemical kinetics. These CPU times, in combination with the relative speeds of various computers given in Table 1 of Ref. [17], show that the time required to advance the EFM solution by one time step, with the single reaction, is slightly less than the reported times for other solution methods for the Euler equations alone (for example Refs. [18–20]) which makes EFM about twice as fast as those methods at each time step. However, the slow approach to steady state in EFM means a larger overall CPU time could be needed to obtain an acceptable approximation to the steady state. This may make EFM as it stands computationally expensive if steady state solutions only are required, although, as mentioned in the Introduction, the robustness of the method may be more important than its speed. It should be remembered that EFM is in its infancy and methods for reducing the computer time, such as local time stepping and adaptive grid techniques [21], could well improve the computational efficiency of EFM.

7. Conclusions

Pullin's equilibrium flux method has been adapted to calculate the flow of a chemically reacting gas where the reaction rates are such that the chemical com-

position is not necessarily in equilibrium with the local density and temperature of the gas. The one-dimensional calculations made with the method show that as the cell size is decreased the EFM results approach the solution obtained from an accurate numerical integration of the governing equations behind a shock in a reacting gas. Calculations of the hypersonic flow of a dissociating gas about a two-dimensional blunt body agree well with previously published results despite the use of a rather coarse computational grid relative to the characteristic reaction length of the flow. The method is robust and has been shown to give results which are virtually independent of the time step used to advance the solution. Like any method which smears discontinuities over a few cells, the results cannot be entirely independent of the grid spacing, yet it has been shown here for a particular case that doubling the number of cells had very little effect on the flowfield and negligible effect on the integrated body forces predicted. There is nothing in the method which limits it to one chemical reaction or the simplified reaction model used here. The only constraint is the computing time required. The two-dimensional calculations with a single chemical reaction did not require a prohibitive amount of computational power.

The equilibrium flux method is not restricted to any particular flow geometry and the core of the method, the calculation of fluxes across cell boundaries, is the same in one, two, or three space dimensions. To extend the method to three dimensions is, therefore, not a problem of fluid mechanics or physics but only a problem of devising an appropriate 3D cell network; although this may not be trivial. Another useful feature of the method is that it becomes an upwind method in the hypersonic limit. This is important because it is in supersonic and hypersonic flows that the flow energy is great enough to initiate chemical reactions in air. The pseudo-dissipative nature of EFM, which detracts somewhat from the accuracy of the method, does, however, appear to make the method robust. The pseudo-dissipation produces no unphysical oscillations which could have disastrous effects on sensitive chemical reactions. These features of EFM make it a promising candidate for the calculation of the fully three-dimensional flow of a reacting gas about a hypersonic cruise or re-entry vehicle.

APPENDIX: Dissipative Effects

A finite volume method for the Euler equations, such as Jameson's [22], is derived from the Euler equations in integral form; that is,

$$\frac{\partial}{\partial t}\int_{\Omega} \mathbf{W}\, d\Omega + \int_{S} \mathbf{F}\cdot\mathbf{n}\, dS = 0, \tag{A.1}$$

where Ω denotes a fixed region with boundary S. The outer normal to the boundary is $\mathbf{n}$, $\mathbf{W}$ is the vector of conserved quantities, and $\mathbf{F}$ is the corresponding flux

tensor. For a one-dimensional flow in a stream tube of constant cross section these are

$$\mathbf{W} = \begin{bmatrix} \rho \\ \rho u \\ \rho E \end{bmatrix}, \qquad \mathbf{F} = \begin{bmatrix} \rho u \\ \rho u^2 + p \\ \rho u(\frac{1}{2}u^2 + c_p T) \end{bmatrix}, \tag{A.2}$$

where p is the pressure. The region $d\Omega$ will be an infinitesimal length of the tube and may be approximated by a discrete cell of volume V_i. Then the Euler equations can be approximated as

$$\frac{d}{dt} V_i \mathbf{W}_i + \mathbf{Q}_i = 0, \tag{A.3}$$

where $\mathbf{Q}_i$ is the net flux out of the ith cell in unit time. This is given by

$$\mathbf{Q}_i = [\mathbf{F}_{i+1/2} - \mathbf{F}_{i-1/2}] \cdot \mathbf{S}, \tag{A.4}$$

where $\mathbf{S}$ denotes the surface area of the two boundaries of the cell and $\mathbf{F}_{i+1/2}$ and $\mathbf{F}_{i-1/2}$ are the flux terms at these boundaries. The boundary fluxes can be approximated by the mean of the fluxes evaluated at the cell centroids either side of the boundary. Thus

$$\mathbf{F}_{i+1/2} = \tfrac{1}{2}[\mathbf{F}_i + \mathbf{F}_{i+1}], \tag{A.5}$$

where

$$F_i = \begin{bmatrix} \rho_i u_i \\ \rho_i u_i^2 + p_i \\ \rho_i u_i(\frac{1}{2}u_i^2 + c_p T_i) \end{bmatrix}. \tag{A.6}$$

In practice, a finite difference solution of Eq. (A.3) will be unable to represent shocks [23]. By adding an "artificial viscosity" [24] or other [22] dissipative terms, $\mathbf{D}$, so that the equation that is solved is

$$\frac{d}{dt} V_i \mathbf{W}_i + (\mathbf{Q}_i - \mathbf{D}_i) = 0, \tag{A.7}$$

the shocks are smeared over a few computational grid points, and a steady solution including the "shock" is achieved.

In EFM $V_i \mathbf{W}_i$ is changed in one time step by an amount

$$\Delta(V_i \mathbf{W}_i) = -\mathbf{Q}_i' \, \Delta t,$$

where

$$Q_i' = [\mathbf{F}_{i+1/2}' - \mathbf{F}_{i-1/2}'] \cdot \mathbf{S} \tag{A.8}$$

is the net flux out of the ith cell in unit time, and $\mathbf{F}'$ is the net flux per unit area in unit time across a cell boundary. In other words, EFM provides an approximate solution of the equation

$$\frac{d}{dt} V_i \mathbf{W}_i + \mathbf{Q}'_i = 0. \tag{A.9}$$

To compare this with (A.7), put $\mathbf{Q}' = \mathbf{Q} - \mathbf{D}'$, where $\mathbf{D}'$ is the equivalent pseudo-dissipative terms in EFM. It follows from (A.4) and (A.8) that

$$\mathbf{D}'_i = \mathbf{d}_i \cdot \mathbf{S} = [\Delta \mathbf{F}_{i+1/2} - \Delta \mathbf{F}_{i-1/2}] \cdot \mathbf{S}, \tag{A.10}$$

where

$$\Delta \mathbf{F}_{i+1/2} = \mathbf{F}_{i+1/2} - \mathbf{F}'_{i+1/2} \tag{A.11}$$

is the difference between the boundary flux of (A.5) and the boundary flux for EFM which can be evaluated from Eqs. (3) in the main text using the conditions in the cells on either side of the boundary. After lengthy algebraic manipulation it is found that

$$\mathbf{F}'_{i+1/2} = \tfrac{1}{2} M_i \mathbf{F}_i + \tfrac{1}{2} N_{i+1} \mathbf{F}_{i+1} - A_i \mathbf{C}_i + A_{i+1} \mathbf{C}_{i+1}, \tag{A.12}$$

where

$$\begin{aligned} M_i &= 1 + 2A_i + 2B_i \\ N_i &= 1 - 2A_i - 2B_i \\ A_i &= \exp(-s_i^2)/(2s_i \pi^{1/2}) \\ B_i &= \operatorname{erf}(s_i)/2 \end{aligned}$$

and

$$\mathbf{C}_i = \begin{bmatrix} 0 \\ p_i \\ \frac{1}{2} u_i p_i \end{bmatrix}.$$

It follows from (A.5), (A.11), and (A.12) that the form of $\Delta \mathbf{F}$ for EFM is

$$\Delta \mathbf{F}_{i+1/2} = \{(A_{i+1} + B_{i+1}) \mathbf{F}_{i+1} - A_{i+1} \mathbf{C}_{i+1}\} - \{(A_i + B_i) \mathbf{F}_i - A_i \mathbf{C}_i\}. \tag{A.13}$$

The pseudo-dissipation can be found from (A.10) and (A.13). It is

$$\begin{aligned} \mathbf{d}_i = {} & \{(A_{i+1} + B_{i+1}) \mathbf{F}_{i+1} - A_{i+1} \mathbf{C}_{i+1}\} - 2\{(A_i + B_i) \mathbf{F}_i - A_i \mathbf{C}_i\} \\ & + \{(A_{i-1} + B_{i-1}) \mathbf{F}_{i-1} - A_{i-1} \mathbf{C}_{i-1}\}, \end{aligned} \tag{A.14}$$

which is the finite difference approximation to a term of the form

$$\mathbf{d} = \frac{\partial^2}{\partial x^2}\left[(A+B)\mathbf{F} - A\mathbf{C}\right].$$

It is interesting to find the hypersonic limit of (A.12). For $s \to \infty$, $A_i \to 0$, $B_i \to \frac{1}{2}$, $N_i \to 0$, and $M_i \to 2$, so

$$\lim_{s \to \infty} \mathbf{F}'_{i+1/2} = \mathbf{F}_i. \tag{A.15}$$

Thus the scheme reduces to a simple up-wind method in which the boundary flux depends only on the conditions on one side of the boundary.

ACKNOWLEDGMENT

I thank Dr. D. I. Pullin for many helpful discussions during the course of this work.

REFERENCES

1. D. I. PULLIN, *J. Comput. Phys.* **34**, 231 (1980).
2. R. D. REITZ, *J. Comput. Phys.* **42**, 108 (1981).
3. S. M. DESPHANDE, *AIAA Paper* 86-0275, Jan. (1986).
4. J. B. GREENBERG AND C. PRESSER, *J. Comput. Phys.* **40**, 361 (1981).
5. W. C. GEAR, *Initial Value Problems in Ordinary Differential Equations* (Prentice-Hall, Englewood Cliffs, NJ, 1971).
6. A. B. WARDLAW, F. P. BALTAKIS, F. M. MARTIN, F. J. PRIOLO, AND R. U. JETTMAR, *J. Spacecraft* **24**, 40 (1987).
7. G. A. BIRD, *Molecular Gas Dynamics* (Oxford Univ. Press (Clarendon), Oxford, 1976).
8. G. A. BIRD, *Phys. Fluids* **13**, 2676 (1970).
9. M. J. LIGHTHILL, *J. Fluid Mech.* **2**, 1 (1957).
10. N. C. FREEMAN, *J. Fluid Mech.* **4**, 407 (1958).
11. W. G. VINCENTI AND C. H. KRUGER, *Physical Gas Dynamics*, reprint (Krieger, Huntington, NY, 1977).
12. G. E. FORSYTHE, M. A. MALCOLM, AND C. B. MOLER, *Computer Methods for Mathematical Computations* (Prentice-Hall, Englewood Cliffs, NJ, 1977).
13. J. A. LORDI, R. E. MATES, AND J. R. MOSELLE, N.A.S.A Current Rep. CR-472, 1965.
14. H. G. HORNUNG, *J. Fluid Mech.* **53**, 149 (1972).
15. L. J. GARR AND P. V. MARRONE, Cornell Aeronaut. Lab. Rep. QM-1626-A-12, II, 1963.
16. N. R. MUDFORD AND R. J. STALKER, *Aero Q.* **31**, 113 (1980).
17. J. J. DONGARRA, *Simulation* **49**, 51 (1987).
18. G. MORETTI, *AIAA Paper* 87-0352 (1987).
19. D. A. CAUGHEY, *AIAA Paper* 87-0354 (1987).
20. L. E. ERIKSSON, *Comput Meth. Appl. Mech. Eng.* **64**, 79 (1987).
21. E. PEREZ, J. PERIAUX, J. P. ROSENBLUM, B. STOUFFLET, A. DERVIEUX, AND M. H. LALLEMAND, in *Tenth Intl. Conf. Num. Methods in Fluid Dynamics*, Lecture Notes in Phys. Vol. 264 (Springer-Verlag, Berlin/New York, 1986).
22. A. JAMESON, W. SCHMIDT, AND E. TURKEL, *AIAA Paper* 81-1259 (1981).
23. P. L. ROE, *Annu. Rev. Fluid Mech.* **18**, 337 (1986).
24. J. VON NEUMANN AND R. D. RICHTMYER, *J. Appl. Phys.* **21**, 232 (1950).